JOURNAL OF MATERIALS SCIENCE 29 (1994) 2754–2760

Stress distribution in discontinuous fibres in a model composite

SHOJIRO OCHIAI, MASAKI HOJO
Mesoscopic Materials Research Center, Faculty of Engineering, Kyoto University, Kyoto 606, Japan

In order to calculate stress distribution in unidirectional discontinuous fibres embedded in a metal matrix, a method based on the shear-lag analysis was proposed. Using this method, the influence of fibre length, interfacial bonding strength, distance between fibre ends in the longitudinal direction, and applied strain to composite on both stress distribution and average stress of fibres was estimated for a number of examples.

1. Introduction

When discontinuous fibres are embedded in metal matrix composites, the stress in the fibres is built up through the shear stress at interface τ. Noting the distance from the fibre end as x, the stress of fibre as $\sigma_f(x)$, and the diameter of fibres as d, the relation of $\sigma_f(x)$ to τ is given by [1]

$$d\sigma_f(x)/dx = (4/d)\tau \quad (1)$$

If τ is taken as a constant, $\sigma_f(x)$ can be given by

$$\sigma_f(x) = (4/d)\tau x \quad (2)$$

and critical length l_c [1], which is a necessary length for the fibres to carry the stress equal to their full strength σ_{fu} at the centre of the length, is given by

$$l_c/d = \sigma_{fu}/(2\tau) \quad (3)$$

Equation 3 has been widely used for analysis of strength of discontinuous fibre-reinforced metal matrix composites by substituting shear yield stress of matrix τ_y, or shear strength τ_u, into τ in the case of high interfacial bonding strength. However, according to studies on stress distribution in broken fibres in originally continuous single-fibre composites with high interfacial bonding [2, 3], τ is not necessarily constant and the stress distribution depends on the applied stress (or strain) level, yield stress and strain hardening rate of the matrix, and the volume fraction of the fibres. In multi-discontinuous-fibre composites, the stress distribution will be affected by the above factors, and also by the distance between the ends of two fibres. Furthermore, it is expected that if interfacial bonding is low, the distribution will be different. The aim of the present work is to present a calculation method for the stress distribution in multi-discontinuous fibres embedded in a strain hardenable metal matrix, by employing a two-dimensional model composite with a simple geometry, and to calculate the stress distribution for some examples.

2. Calculation method

2.1. Model composite

In the present attempt to calculate stress distribution, a two-dimensional model composite as shown in Fig. 1 was employed. In the model, the fibres with length l and width d_f are assumed to be embedded regularly in longitudinal rows. The distance between fibre ends in each longitudinal row is given by $2a$ in Fig. 1. The fibre rows are described as "1" and "2", which exist alternately such that the centre of length in the fibres in row 1 exists in the cross-section where the centre of fibre ends in row 2 exists, as shown in Fig. 1.

As the fibres exist regularly in this model, the region surrounded by the broken line in Fig. 1 was picked up and the equations for stress equalibrium were given for this representative region. The centre of the fibres in row 2 was taken as $x = 0$, and the fibre end in row 1 was given as $x = a$.

From the geometry shown in Fig. 1, the width of matrix d_m for $a < x < l/2$ was given by

$$d_m = d_f[l(l - V_f) - 2aV_f]/[V_f(l + 2a)] \quad (4)$$

where V_f is the volume fraction of fibres.

2.2. Approximations

In the present work, shear-lag analysis was employed, which has been widely used to calculate stress distribution in broken and neighbouring fibres in multi-continuous fibre composites [4–9]. The following approximations were made for simplicity.

(i) The composite is composed of tension-carrying fibres embedded in a shear-carrying matrix, which plays a role only as the stress-transfer medium. This approximation is common in shear-lag-analysis [4–9].

(ii) The stress in the transverse direction is neglected. This approximation is also common in shear-lag analysis.

(iii) The shear stress τ_m-shear strain γ curve of the matrix is composed of an elastic region for $\gamma < \gamma_y$ where γ_y is the yield strain in shear and that of a plastic region for $\gamma > \gamma_y$ where matrix work-hardens linearly with respect to strain. Under this approximation, the τ_m is given by

$$\tau_m = G_m\gamma \quad (5)$$

0022–2461

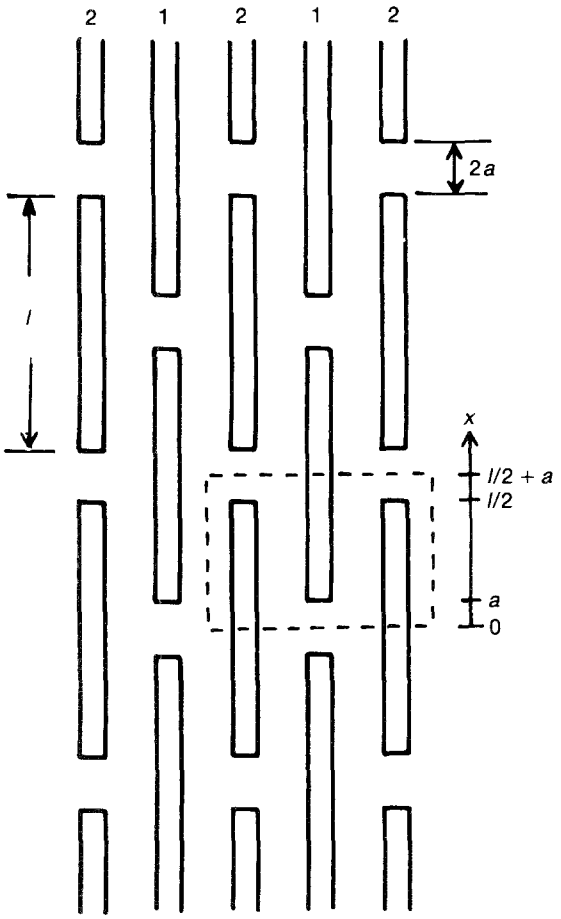

Figure 1 Geometry of the model employed in the present work.

for $\gamma < \gamma_y$ where G_m is the shear modulus of the matrix, and

$$\tau_m = (1 - \beta)\tau_y + \beta G_m \gamma \quad (6)$$

for $\gamma > \gamma_y$ where τ_y is the shear yield stress given by $G_m\gamma_y$ and β is the slope of the shear stress–strain curve in the plastic region, normalized with respect to G_m.

2.3. Deformation stages

Yielding of the matrix and interfacial debonding can occur, dependent on the applied strain e. A schematic representation of the occurrence of these events is shown in Fig. 2, which represents the region surrounded by the broken line in Fig. 1.

When the applied strain e is low, the matrix deforms elastically (stage a in Fig. 2a). With increasing applied strain, the shear stress at interface τ increases and the matrix becomes plastic (b) if $\tau_i > \tau_y$ where τ_i is the interfacial bonding strength in shear; or interfacial debonding arises if $\tau_y > \tau_i(c)$. With further increasing strain, the range of plastic deformation ($a < x < a + b$ and $l/2 - b < x < l/2$) in (b), or that of interfacial debonding ($a < x < c$ and $l/2 - c < x < l/2$) in (c) increases, where b and c are lengths of the region where matrix behaves plastically and the region where interfacial debonding occurs, respectively.

For stage b, there are two possible stages after further straining. If no interfacial debonding occurs, stage b reaches $l/2(d)$, but if debonding occurs before

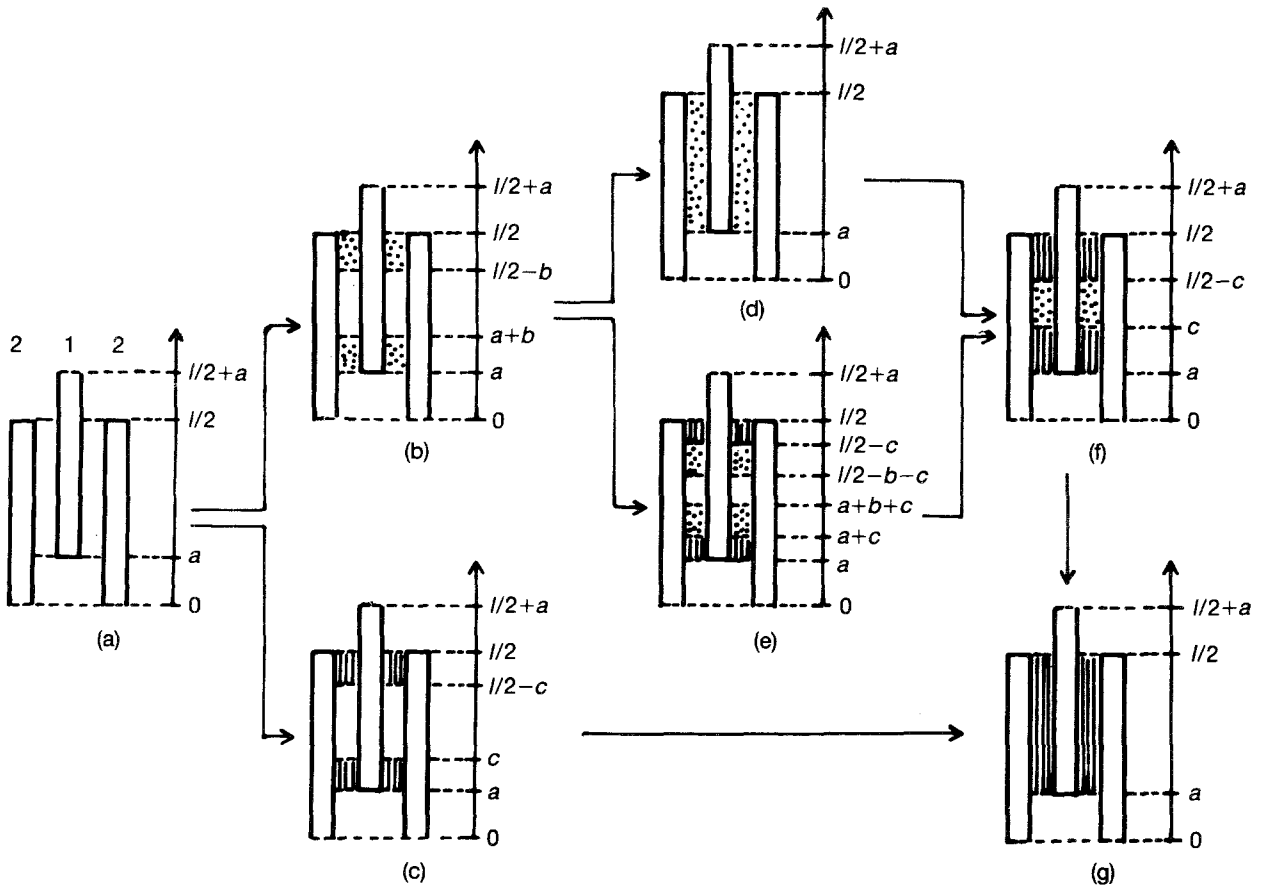

Figure 2 Schematic representation of deformation stages. □, ▦ and ▥ shown in the matrix areas refer to the regions where matrix behaves elastically, matrix behaves plastically and interfacial debonding occurs, respectively.

stage b reaches $l/2$, stage e arises. Once stage c has occurred, the region of debonding grows and stage c reaches $l/2(g)$. When stage d has occurred, the shear stress at the interface increases with increasing applied strain, and a region of debonding arises (f). When stage e has occurred, the regions of plastic matrix and interfacial debonding grow and the region of elastic matrix disappears upon further straining, resulting in stage f. When stage f has occurred, the region of debonding grows with increasing strain and the region of plastic matrix disappears (stage g).

There are seven possible stages as stated above. Which stage appears is dependent on the volume fraction of the fibre, elastic properties of both fibres and matrix, plastic properties of the matrix, interfacial bonding strength, and fracture strain of composites. For instance, if the interfacial bonding strength is high enough to suppress debonding, only stages a, b and d arise. Furthermore, if the composite fractures before stage d appear, only stages a and b appear for low and high applied strains, respectively.

2.4. Equations of stress equilibrium

Here, stage e is taken as an example and equations of stress equilibrium are presented, as this stage contains all kinds of regions (elastic matrix, plastic matrix and interfacial debonding). For simplicity, the regions for $0 < x < a$, $a < x < a + c$, $a + c < x < a + b + c$, $a + b + c < x < l/2 - b - c$, $l/2 - b - c < x < l/2 - c$, $l/2 - c < x < l/2$ and $l/2 < x < l/2 + a$ are named as regions A to G, respectively.

Noting the displacement of the "1" and "2" fibres as u_1 and u_2, respectively, the shear stress τ is expressed as

$$\tau = (G_m/d_m)(u_1 - u_2) \tag{7}$$

when the matrix behaves elastically, and it is expressed as

$$\tau = (1 - \beta)\tau_y + (\beta G_m/d_m)(u_1 - u_2) \tag{8}$$

when the matrix behaves plastically. When interfacial debonding has occurred, τ is given by

$$\tau = \tau_f \tag{9}$$

where τ_f is the frictional shear stress acting at the interface after debonding. In the range of $0 < x < a$ and $l/2 < x < l/2 + a$, τ is given by

$$\tau = 0 \tag{10}$$

as the u_2 of the "2" fibres surrounding the "1" fibres is the same.

Noting the Young's modulus of fibres as E_f, the following equations for stress equilibrium can be given for regions A to G.

regions A and G:

$$d_f E_f(d^2u_2/dx^2) = 0 \tag{11}$$

regions B and F:

$$d_f E_f(d^2u_1/dx^2) = 2\tau_f \tag{12}$$

$$d_f E_f(d^2u_2/dx^2) = -2\tau_f \tag{13}$$

regions C and E:

$$d_f E_f(d^2u_1/dx^2) = 2[(1 - \beta)\tau_y + (\beta G_m/d_m)(u_1 - u_2)] \tag{14}$$

$$d_f E_f(d^2u_2/dx^2) = -2[(1 - \beta)\tau_y - (\beta G_m/d_m)(u_1 - u_2)] \tag{15}$$

region D:

$$d_f E_f(d^2u_1/dx^2) = 2[(G_m/d_m)(u_1 - u_2)] \tag{16}$$

$$d_f E_f(d^2u_2/dx^2) = -2[(G_m/d_m)(u_1 - u_2)] \tag{17}$$

2.5. General solutions

By solving Equations 11 to 17, the solutions for regions A to G are given by

region A:

$$u_2^A = A_1x + A_2 \tag{18}$$

region B:

$$u_1^B = \tau_f x^2/(d_f E_f) + B_1x + B_2 \tag{19}$$

$$u_2^B = -\tau_f x^2/(d_f E_f) + B_3x + B_4 \tag{20}$$

region C:

$$u_1^C = [d_f d_m E_f/(4\beta G_m)](C_1 \cosh\{[4\beta G_m/(d_f d_m E_f)]^{1/2}x\} + C_2 \sinh\{[4\beta G_m/(d_f d_m E_f)]^{1/2}x\}) + C_3x + C_4 \tag{21}$$

$$u_2^C = [(1 - \beta)d_m\tau_y/(\beta G_m)] - [d_f d_m E_f/(4\beta G_m)] \times (C_1 \cosh\{[4\beta G_m/(d_f d_m E_f)]^{1/2}x\} + C_2[\sinh\{[4\beta G_m/(d_f d_m E_f)]^{1/2}x\}) + C_3x + C_4 \tag{22}$$

region D:

$$u_1^D = [d_f d_m E_f/(4G_m)](D_1 \cosh\{[4G_m/(d_f d_m E_f)]^{1/2}x\} + D_2 \sinh\{[4G_m/(d_f d_m E_f)]^{1/2}x\}) + D_3x + D_4 \tag{23}$$

$$u_2^D = -[d_f d_m E_f/(4G_m)](D_1 \cosh\{[4G_m/(d_f d_m E_f)]^{1/2}x\} + D_2 \sinh\{[4G_m/(d_f d_m E_f)]^{1/2}x\}) + D_3x + D_4 \tag{24}$$

region E:

$$u_1^E = [d_f d_m E_f/(4\beta G_m)]\{E_1 \cosh[4\beta G_m/(d_f d_m E_f)]^{1/2}x\} + E_2 \sinh\{[4\beta G_m/(d_f d_m E_f)]^{1/2}x\} + E_3x + E_4 \tag{25}$$

$$u_2^E = [(1 - \beta)d_m\tau_y/(\beta G_m)] - [d_f d_m E_f/(4\beta G_m)] \times (E_1 \cosh\{[4\beta G_m/(d_f d_m E_f)]^{1/2}x\} + E_2 \sinh\{[4\beta G_m/(d_f d_m E_f)]^{1/2}x\}) + E_3x + E_4 \tag{26}$$

region F:

$$u_1^F = \tau_f x^2/(d_f E_f) + F_1x + F_2 \tag{27}$$

$$u_2^F = -\tau_f x^2/(d_f E_f) + F_3x + F_4 \tag{28}$$

region G:

$$u_1^G = G_1 x + G_2 \quad (29)$$

The superscripts A to G of u_i refer to regions A to G, respectively.

2.6. Boundary conditions

The boundary conditions to solve the integral constants A_i and $G_i (i = 1$ and 2), B_i, C_i, D_i, E_i and F_i ($i = 1$ to 4), and the lengths b and c (total 26 unknown values) are given as follows.

(1) At any cross-section, the applied load is constant.

$$du_2^A/dx = du_1^B/dx + du_2^B/dx \quad (30)$$

$$du_1^B/dx + du_2^B/dx = du_1^C/dx + du_2^C/dx \quad (31)$$

$$du_1^C/dx + du_2^C/dx = du_1^D/dx + du_2^D/dx \quad (32)$$

$$du_1^D/dx + du_2^D/dx = du_1^E/dx + du_2^E/dx \quad (33)$$

$$du_1^E/dx + du_2^E/dx = du_1^F/dx + du_2^F/dx \quad (34)$$

$$du_1^F/dx + du_2^F/dx = du_1^G/dx \quad (35)$$

(2) From the geometry of the present model, the stress in "1" fibres at $x = z$ (z: arbitrary value less than $l/4 + a/2$) is equal to the stress in "2" fibres at $x = l/2 + a - z$.

$$(du_1^B/dx)_z = (du_2^F/dx)_{l/2+a-z} \quad (36)$$

$$(du_1^C/dx)_z = (du_2^E/dx)_{l/2+a-z} \quad (37)$$

$$(du_1^D/dx)_z = (du_2^D/dx)_{l/2+a-z} \quad (38)$$

From Equations 30 to 38, the conditions that

$$(du_1^E/dx)_z = (du_2^C/dx)_{l/2+a-z}$$

$$(du_1^F/dx)_z = (du_2^B/dx)_{l/2+a-z}$$

$$(du_1^G/dx)_z = (du_2^A/dx)_{l/2+a-z}$$

are satisfied automatically.

(3) At any x, the displacement should be continuous.

$$u_1^B(a + c) = u_1^C(a + c) \quad (39)$$

$$u_1^C(a + b + c) = u_1^D(a + b + c) \quad (40)$$

$$u_1^D(l/2 - b - c) = u_1^E(l/2 - b - c) \quad (41)$$

$$u_1^E(l/2 - c) = u_1^F(l/2 - c) \quad (42)$$

$$u_1^F(l/2) = u_1^G(l/2) \quad (43)$$

$$u_2^A(a) = u_2^B(a) \quad (44)$$

$$u_2^B(a + c) = u_2^C(a + c) \quad (45)$$

$$u_2^C(a + b + c) = u_2^D(a + b + c) \quad (46)$$

$$u_2^D(l/2 - b - c) = u_2^E(l/2 - b - c) \quad (47)$$

$$u_2^E(l/2 - c) = u_2^F(l/2 - c) \quad (48)$$

(4) At $x = 0$, the displacement of "2" fibres is zero.

$$u_2^A(0) = 0 \quad (49)$$

(5) The applied strain, e, is related to

$$e = u_1^G(l/2 + a)/(l/2 + a) \quad (50)$$

(6) At $x = a + c$ and $l/2 - c$, interfacial debonding occurs.

$$\tau_i = (1 - \beta)\tau_y + \beta G_m[u_1^C(a + c) - u_2^C(a + c)]/d_m \quad (51)$$

The condition that

$$\tau_i = (1 - \beta)\tau_y + \beta G_m[u_1^E(l/2 - c) - u_2^E(l/2 - c)]/d_m$$

is satisfied automatically from conditions 1 and 2 and Equation 51.

(7) At $x = a + b + c$ and $l/2 - b - c$, yielding of matrix in shear occurs.

$$\tau_y = G_m[u_1^D(a + b + c) - u_2^D(a + b + c)]/d_m \quad (52)$$

The condition that

$$\tau_y = G_m[u_1^D(l/2 - b - c) - u_2^D(l/2 - b - c)]/d_m$$

is satisfied automatically from conditions 1 and 2, and Equation 52.

(8) At $x = a$, the stress of "2" is zero.

$$(du_1^B/dx)_a = 0 \quad (53)$$

(9) At any x, the stress in fibres should be continuous.

$$(du_1^B/dx)_{a+c} = (du_1^C/dx)_{a+c} \quad (54)$$

$$(du_1^C/dx)_{a+b+c} = (du_1^D/dx)_{a+b+c} \quad (55)$$

The conditions that the stress in "1" is continuous at $x = l/2 - b - c$, $l/2 - c$, and $l/2 + a$, and that the stress in "2" is continuous at $x = a$, $a + c$, $a + b + c$, $l/2 - b - c$ and $l/2 - c$, are satisfied automatically from conditions 1 and 2 and Equations 54 and 55.

In the calculation, e was given step by step, the unknown values were calculated and then the distribution of stress as a function of x, σ_f, was calculated from $E_f(du_1/dx)$, and the shear stress at interface τ from Equations 7–9. The average stress of fibres, $\bar{\sigma}_f$, was calculated from

$$\bar{\sigma}_f = (1/l)\int_0^l \sigma_f dl \quad (56)$$

As stated above, the stress distribution can be calculated for stage e. For other stages, it can be calculated in a similar manner.

3. Results and discussion

In the present calculation, the following values were used: $E_f = 400$ GPa, $G_m = 40$ GPa, $\tau_y = 100$ MPa, $\tau_f = 20$ MPa, $\beta = 0.02$, $V_f = 0.5$, $d_f = 10$ μm, $\tau_i = 300$ and 120 MPa, $l = 250$ and 500 μm, $2a = 0$ to 400 μm and $e = 0$ to 2%.

3.1. Variation of interfacial shear stress at fibre-end as a function of applied strain to composite

The shear stress was highest at $x = a$, as will be shown in 3.2 below. Fig. 3 shows some examples of the variation of $\tau(a)$ as a function of applied strain e for $\tau_i = 300$ MPa, which was high enough to suppress

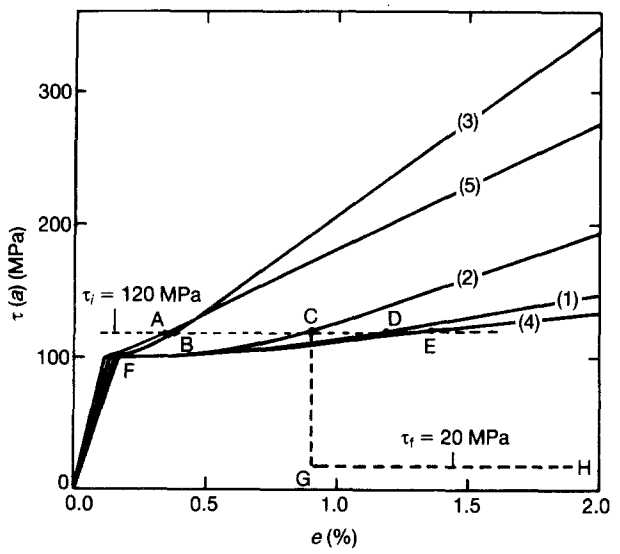

Figure 3 Variations of interfacial shear stress at $x = a$, $\tau(a)$ as a function of strain of composite, e, for $\tau_i = 300$ MPa (solid curves) and for $\tau_i = 120$ MPa (broken curve for (2)) for comparison. l = (1) 500; (2) 500; (3) 500; (4) 250; (5) 250 μm. $2a$ = (1) 0; (2) 200; (3) 400; (4) 0; (5) 200 μm.

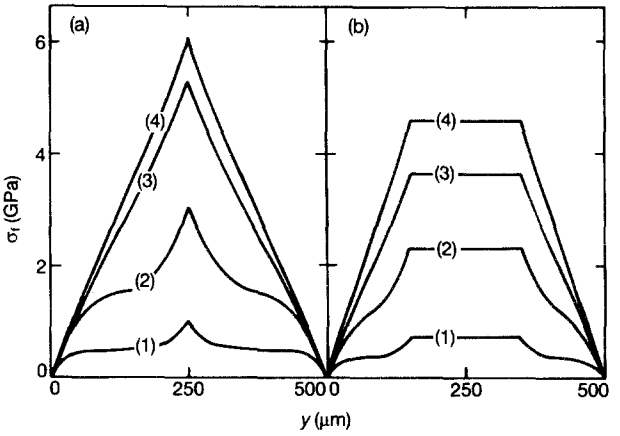

Figure 4 Distribution of stress in fibres, σ_f, as a function of distance from the fibre end, y, at various strain levels, under conditions of $l = 500$ μm; $\tau_i = 300$ MPa. e = (1) 0.15; (2) 0.50; (3) 1.0; (4) 1.5. $2a$ = (a) 0; (b) 200 μm.

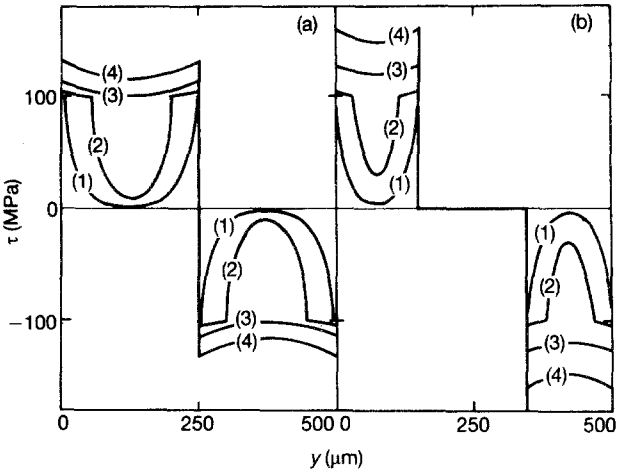

Figure 5 Distribution of shear stress at interface, τ, as a function of distance from the fibre end, y, under conditions of $l = 500$ μm; $\tau_i = 300$ MPa and $2a$ = (a) 0 and (b) $2a$ 200 μm. The curves (1) to (4) correspond to (1) to (4) in Fig. 4, respectively.

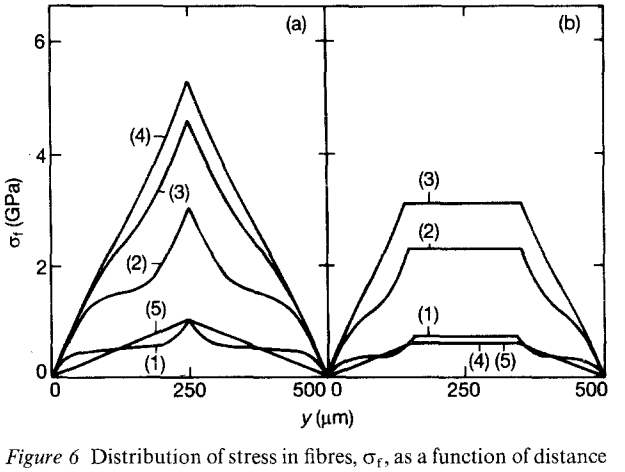

Figure 6 Distribution of stress in fibres, σ_f, as a function of distance from the fibre end, y, at various strain levels, under conditions of (a) $l = 500$ μm; $\tau_i = 120$ MPa, and $2a$ = (a) 0 and (b) $2a$ 200 μm; l = (1) 0.15; (2) 0.50; (3) 0.85; (4) 1.0; (5) 1.20.

interfacial debonding for $e < 2\%$. The values of l and $2a$ used for the calculation are given in the caption to Fig. 3. Two distinct features can be read from Fig. 3.

(i) The $\tau(a)$ increases with increasing e linearly in the elastic stage of the matrix (stage a), but when e becomes large and plastic deformation of the matrix occurs, it increases with increasing e rather slowly. However, the increasing rate of $\tau(a)$ with respect to e in the plastic stage of the matrix becomes high at high e due to strain-hardening of the matrix.

(ii) When 2a is small ((1) and (2)) in Fig. 3, the increase in $\tau(a)$ in the plastic stage of matrix is low, while when $2a$ is large in comparison with l ((3) and (5)), it is high: namely in the case of large $2a/l$, the interfacial shear stress at $x = a$ becomes very high, especially at high e.

When $\tau(a)$ exceeds τ_i, interfacial debonding arises. Taking the case of $\tau_i = 120$ MPa as an example, interfacial debonding occurs at D, C, B, E and A for (1) to (5) in Fig. 3, respectively. Once debonding occurs, the $\tau(a)$ becomes equal to τ_f. As a result, $\tau(a)$ varies along OFCGH for (2). As the $\tau(a)$ reaches τ_i at small strain e when $2a/l$ is large, debonding occurs at small e and the efficiency of stress transfer to fibres is reduced. This point will be discussed in detail in 3.3 below.

3.2. Tensile and shear stress distributions as a function of distance from the fibre end

Tensile stress distribution in fibres σ_f and shear stress distribution τ at the interface for $\tau_i = 300$ MPa were calculated as shown in Figs 4 and 5, respectively, and those for $\tau_i = 120$ MPa in Figs 6 and 7, respectively. (a) and (b) in Figs 4 to 7 show the cases of $2a = 0$ and 200 μm, respectively. When $\tau_i = 300$ MPa, there occurred no interfacial debonding up to $e = 2\%$, but when τ_i was 120 MPa, there occurred debonding for $e > 1.2\%$ for $2a = 0$ and for $e > 0.88\%$ for $2a = 200$ μm. In the case of $\tau_i = 300$ MPa (Figs 4 and 5), $e = 0.15$, 0.50, 1.0 and 1.5% for $2a = 0$, corresponding to the stages a, b, d and d, respectively, and those for $2a = 200$ μm to the stages b, b, d and d, respectively. In case of $\tau_i = 120$ MPa (Figs 6 and 7),

$e = 0.15$, 0.50, 0.85, 1.00 and 1.2% for $2a = 0$, corresponding to the stages a, b, d, d and g, respectively, and those for $2a = 200$ μm to the stages b, d, d, g and g, respectively. The y in Figs 4 to 7 shows the distance from the end of the fibres.

From the geometry of the present model, the stress distribution in "1" fibres as a function of y was equal to that in "2" fibres, and also the stress distribution in fibres was symmetrical with respect to the centre of $y = l/2$. The variation of $\tau(y)$ was equal to $-\tau(l/2 - y)$ due to the geometry of the present model, and also the $\tau(y)$ was symmetrical with respect to $y = (l - 2a)/4$ for $0 < y < l/2 - a$ and also with respect to $y = (3l + 2a)/4$ for $l/2 + a < y < l$. For $l/2 - a < y < l/2 + a$, τ was zero, as stated already. The following features can be seen from Figs 4 to 7.

(i) At any strain, e, the stress σ_f for $2a = 0$ increases with increasing y, and reaches maximum at $x = l/2$(250 μm in this example) and then decreases, while that for $2a = 200$ μm increases and reaches maximum at $y = l/2 - a$, remaining constant for $l/2 - a < y < l/2 + a$.

(ii) The stress distribution for $2a = 0$ is very acute near the centre of the length, but not for $2a = 200$ μm. The highest stress in fibre at $y = l/2$ for $2a = 0$ is higher than that for $2a = 200$ μm. As the breakage of fibres occurs when the exerted stress exceeds their strength, the fibres for $2a = 0$ tend to be broken in comparison with those for large values of $2a$.

(iii) When τ_i is high (300 MPa), the fibre stress σ_f except at $y = 0$ increases with increasing e, whereas when τ is low (120 MPa), the σ_f increases within the range of low e where interfacial debonding does not occur, but decreases at high e due to interfacial debonding.

(iv) τ, except for the range of $l/2 - a < y < l/2 + a$, increases with increasing e when τ_i is high (300 MPa), while it increases but then decreases due to interfacial debonding, remaining constant ($= \tau_f$) at high e when τ_i is low (120 MPa).

3.3. Average stress of fibres as a function of applied strain to composites

Figs 8 and 9 show variations of $\bar{\sigma}_f$ as a function of e for $\tau_i = 300$ and 120 MPa, respectively. The following features can be seen from Figs 8 and 9.

(i) In the case of high τ_i, the $\bar{\sigma}_f$ increases with increasing e, while for low τ_i, it increases within the range of low e where debonding does not arise, but then decreases due to interfacial debonding. The debonding, which occurs at first at $x = a(y = 0)$, propagates quickly and the σ_f is reduced quickly with increasing e, resulting in a quick loss in the stress-carrying capacity of the fibres.

(ii) The increase in $\bar{\sigma}_f$ for $\tau_i = 300$ MPa with increasing e is dependent on the values of l, $2a$ and e. The influence of l on $\bar{\sigma}_f$ is simple: the larger the l, the higher the $\bar{\sigma}_f$. The influence of $2a$ on $\bar{\sigma}_f$ is complex. Comparing (1) with (2) in Fig. 8, for instance, the $\bar{\sigma}_f$ of (2) is higher than that of (1) for $0 < e < 0.8\%$ and $1.2\% < e$, but not for $0.8\% < e < 1.2\%$.

(iii) In the case of low τ_i (120 MPa), debonding arises at lower e for larger $2a$, as the $\tau(a)$ reaches τ_i at lower e, as shown in Fig. 3. Thus the larger the $2a$, the earlier the reduction in $\bar{\sigma}_f$ when τ_i is low. The maximum value of $\bar{\sigma}_f$ increases with increasing l and with decreasing $2a$.

(iv) Once interfacial debonding has occurred in the whole range of y, only τ_f acts to transfer stress to fibres. In such a case, the $\bar{\sigma}_f$ remains constant, being independent of e. The $\bar{\sigma}_f$ after debonding decreases with decreasing l and increasing $2a$.

It should be noted that when τ_i is high, an appropriate selection of $2a$ can produce high composite strength for the following reasons. Taking the case of $l = 500$ μm and $e = 1\%$ in Fig. 8 as an example, (i) the $\bar{\sigma}_f$ of (1) and (2) is higher than that of (3), but (ii) the $\bar{\sigma}_f$ is not so much different between (1) and (2). Too large $2a$ results in low efficiency of stress-transfer (i), and high efficiency of stress-transfer to fibres can be achieved when $2a$ is not too large (ii). Recalling the stress distribution in fibres in Fig. 4, the stress near the centre of the length is acute and very high when

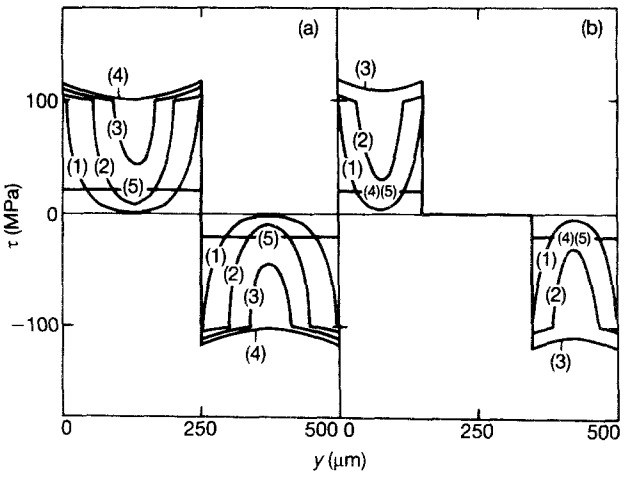

Figure 7 Distribution of shear stress at interface, τ, as a function of distance from the fibre end, y, under a condition of (a) $l = 500$ μm; $\tau_i = 120$ MPa and $2a =$ (a) 0 and (b) 200 μm. The curves (1) to (5) correspond to (1) to (5) in Fig. 6, respectively.

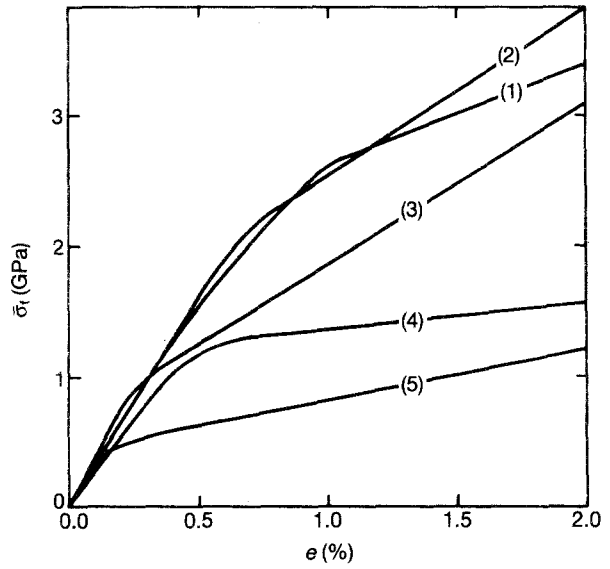

Figure 8 Variation of average fibre stress, $\bar{\sigma}_f$, as a function of strain of composite, e, for various values of l and $2a$ under a condition of $\tau_i = 300$ MPa. $l =$ (1)–(3) 500; (4)–(5) 250 μm. $2a =$ (1) 0; (2) 200; (3) 400; (4) 0; (5) 200 μm.

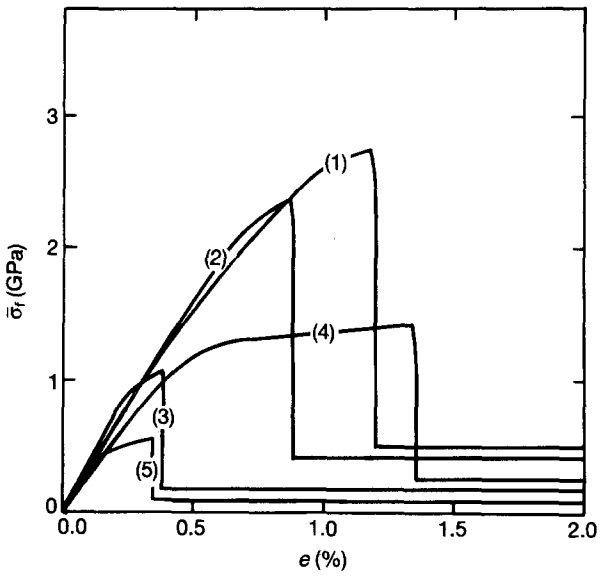

Figure 9 Variation of average fibre stress, $\bar{\sigma}_f$, as a function of strain of composite, e, for various values of l and $2a$, which are the same as those employed for the calculation of Fig. 8, under conditions of $\tau_i = 120$ MPa. l = (1)–(3) 500; (4)–(5) 250 μm. $2a$ = (1) 0; (2) 200; (3) 400; (4) 0; (5) 200 μm.

$2a = 0$, but not when $2a = 200$ μm. This indicates that the breakage of fibres is likely to occur for $2a = 0$ in comparison with that for $2a = 200$ μm, while the average fibre stress is not very different. For instance, taking the strength of fibres to be 4 GPa, the fibres are broken at $e = 1\%$ when $2a = 0$, but not when $2a = 200$ μm. On the other hand, the results for the low τ_i shown in Fig. 9 indicate that the $2a$ should be small in order to achieve high composite strength if the debonding occurs before the stress at $y = l/2$ exceeds the strength of the fibres.

4. Conclusions

The tensile stress distribution in fibres and shear-stress distribution at the interface along the fibre axis, and the average stress carried by the fibres as a function of applied strain in discontinuous fibre-reinforced metal matrix composites, were calculated based on shear-lag analysis using a two-dimensional model with a simple geometry. The influences of fibre length, interfacial bonding strength, distance between fibre ends, and strain applied to composites, on the stress distributions and average stress of fibres, were shown from the results of the calculation.

Acknowledgement

This work was supported in part by the Mazda Foundation research grant.

References

1. A. KEKKY and W. R. TYSON, *J. Mech. Phys. Sol.* **13** (1965) 329.
2. S. OCHIAI and K. OSAMURA, *Z. Metallkd* **77** (1986) 249.
3. *Idem, ibid.* **77** (1986) 255.
4. J. M. HEDGEPETH, *NASA TN D-882* (NASA, Washington DC, 1961).
5. J. M. HEDGEPETH and P. V. DYKE, *J. Comp. Mater.* **1** (1967) 294.
6. C. ZWEBEN, *Eng. Frac. Mech.* **6** (1974) 1.
7. E. D. REEDY, Jr, *J. Mech. Phys. Sol.* **28** (1980) 265.
8. J. G. GOREE and R. S. GROSS, *Eng. Frac. Mech.* **13** (1980) 563.
9. S. OCHIAI, K. ABE and K. OSAMURA, *Z. Metallkd* **76** (1985) 299.

Received 23 September 1992
and accepted 27 September 1993